

FAILURE ANALYSIS AND MECHANICAL BEHAVIOUR OF A60 STEEL BOLLARDS USED IN PORT INFRASTRUCTURE

Mohammed Khalil El Kouifat* and Houcine Zniker

Department of Materials Engineering, The National Higher School of Mining of Rabat (ENSMR),
MOROCCO

E-mail: elkouifatkhalil@gmail.com

Ikram Feddal

Department of Industrial and Civil Sciences and Technologies, Abdelmalek Essaadi Tetouan,
MOROCCO

Bennaceur Ouaki

Department of Materials Engineering, The National Higher School of Mining of Rabat (ENSMR),
MOROCCO

The failure mechanisms and mechanical properties of bollards present significant risks in port and maritime engineering thereby calling for a thorough investigation into these aspects. This study highlights the significance of elements like tensile strength shear stress and service loads while examining the difficulties related to metal bollard failures. This paper presents a case study on A60 steel bollards that combines numerical simulations with experimental testing using Catia and Mathcad software. The results reveal that even as the mechanical houses adjust to A60 steel standards, under accurate ambit and a hundred-ton load, compactness and shear stresses exceed the limit attrition of the bollard. The acceptable strain considerably surpasses the adaptable limit, advertence impending failure. The analysis recommends layout adjustments, presenting a higher array of the annular part of the demonstrated bollard and a safety factor of at least 1.5 to boost the bollard attrition and forestall hurt under a hundred-ton load. This research contributes advantageous insights into bollard layout, acclamation real-global demanding situations, and promoting safety in maritime infrastructure.

Key words: bollard failure, A60 steel bollard; mechanical behaviour; numerical simulation, von Mises stress.

1. Introduction

The phenomenon of metallic bollard failure constitutes a noteworthy apprehension inside the realm of maritime and port engineering. Those structural factors, mainly devised to undergo the mooring and towing forces exerted via vessels, cope with massive loads. Untimely failures in those bollards can precipitate excessive repercussions, encompassing material harm, operational disruptions, and, in the direst instances, jeopardizing the safety of individuals and their surroundings. The evaluation of metal bollard failures requires a complete comprehension of the mechanical traits of the employed materials, the carried out provider masses, and the stresses borne through those additives [1, 2]. Additionally, considerations should extend to factors along with corrosion, fatigue, and the intricacies of structural layout. Practical control of those variables proves indispensable to ensuring the dependability and durability of metal bollards, thereby diminishing the chance associated with unexpected failures and their potentially catastrophic implications [3, 4].

The mechanical properties of substances, specifically in the context of bollards used for port infrastructure, security, and protection, are vital for ensuring their effectiveness and sturdiness. Tensile strength, measuring a fabric's resistance to pulling forces, is vital for bollards, where excessive tensile strength helps face

* To whom correspondence should be addressed

collisions and pressured access tries. Metallic, a common place bollard fabric, is favoured for its extremely good tensile strength. Yield strength is another key issue, representing a material's highest stress tolerance without permanent deformation. In bollards, preventing plastic deformation under applied forces is critical. Impact resistance is good sized as bollards regularly face dynamic masses; a material with desirable impact resistance absorbs and distributes strength, reducing the risk of rupture [5].

Corrosion emerges as a powerful risk to metallic bollards, especially when situated in an out-of-doors environment. Scholars have conducted huge inquiries into strategies aimed at mitigating its deleterious consequences [6-8]. Protective coatings, exemplified by galvanizing, powder coating, and anti-corrosion paints, are characterized as formidable obstacles, fortifying terminals against the encroachments of environmental factors. Monitoring methodologies, along with ultrasonic testing, have the potential to determine corrosion without inducing structural compromise, thus facilitating rapid intervention.

Analysing the given loads, such as mooring forces and ship tension, is critical for knowing the pressure on bollards [9-12]. In response to these loads, design guidelines and standards have been developed to make sure bollards can withstand the tension from ships as well as the dynamic forces of mooring operations. Large navigation vessels, quick lock entries and difficult mooring circumstances – such as irregularities and intricate flow dynamics inside lock chambers – often lead to structural damage or failure of the locks floating bollards as a result of excessive mooring forces. To better understand bollard resistance and their ability to withstand damage under varying dynamic loads a variety of research projects have been undertaken. Wu *et al.* [13] discussed the shortcomings of conventional cable load measurement techniques for floating bollards highlighting the requirement for immediate feedback on the properties of force. The study uses 3D finite element simulations to determine theoretical model parameters for a floating bollard load response using data from a representative ship lock project in China. In a field test, it creates an intelligent monitoring system that integrates big data the internet and cloud services and shows accuracy. According to the previous study [13], ship lock automation and general risk prevention can be improved by implementing a digital perception monitoring platform. Pin *et al.* [14] suggested a novel approach for monitoring mooring bollard structural safety. It determines the relationship between mooring force and surface maximum strain, finds the most unfavourable mooring configuration that maximizes surface stress, and proposes a safety assessment technique based on maximum strain as the threshold value. Using distributed optical fiber sensing technologies, strain values are compared to assess structural safety, providing an accurate and operable technique for mooring bollard monitoring. Sydorenko *et al.* [15, 16] investigated the critical significance of a floating bollard in lock mooring, emphasizing its effect on ship passage organization and operating efficiency. The study uses the finite element approach and 3D modeling to analyze stress-strain states under varied loads, taking into account mooring dynamics and weather conditions. A comparison analysis using a reduced model finds significant stress spots and proposes their usage as sensors in a warning system for the ship lock's floating bollard loading condition.

The examination of actual incidents involving the rupture of metal bollards provides vital insights into the underlying causes and applicable lessons. This empirical technique allows engineers and researchers to identify elements that lead to failures, whether they are related to material weaknesses, design flaws, or environmental constraints. The analysis of such cases allows for a more in-depth understanding of potential vulnerabilities within the industry, providing for the inclusion of corrective measures in future designs or maintenance methods. This proactive integration of knowledge from real experiences is critical for improving the dependability and safety of metal bollards. It ensures that the lessons garnered from past incidents contribute substantively to ongoing enhancements, fostering the evolution of more resilient structures within the field. Consequently, this study undertakes an examination of real-world cases involving the rupture of A60 steel bollards. The investigation encompasses damage analysis and the mechanical behavior of A60 steel bollards utilized in port infrastructure, employing methodologies such as mechanical characterization, simulations via Mathcad, and numerical modelling through Catia.

2. Materials and methods

This paper investigates the actual situation of A60 steel bollards in Morocco's port infrastructure, as shown in Fig.1.



Fig.1. Images of a real-world A60 steel bollard case in port infrastructure.

2.1. Materials

The A60 steel is defined by the AFNOR standard A35-501 with grade 1 or 2 (effervescent or non-effervescent). The correspondence with other international standards is provided in Tab.1:

Table 1. Nomination of bollard steel tested according to international standards.

AFNOR	DIN	NF EN 1027-1
A 60-2	ST 60-2	E335 (1.0060)

A60-2 steel is a non-alloyed, general-purpose construction steel that is non-effervescent and commonly used in general mechanics. In its untreated form, it provides good mechanical strength (tensile strength R_m), and the chemical composition is not defined by the standard and does not guarantee any specific heat treatments. Its characteristics in the normalized state are as follows:

Table 2. Mechanical properties of A60-2 steel tested.

Tensile strength $R_m (N/mm^2)$	Yield strength $R_e (N/mm^2)$	Strain at break $A(\%)$
590-770	305-335	6-16

2.2. Characterization tests of bollard steel

2.2.1. Tensile tests

In order to verify the mechanical properties of such steel, standard tensile test specimens were extracted from the bollard that underwent fracture. An example of a prepared specimen and testing machine for tensile tests are shown in Fig.2. This test method was conducted in accordance with ISO 6892-1 test standard [17].

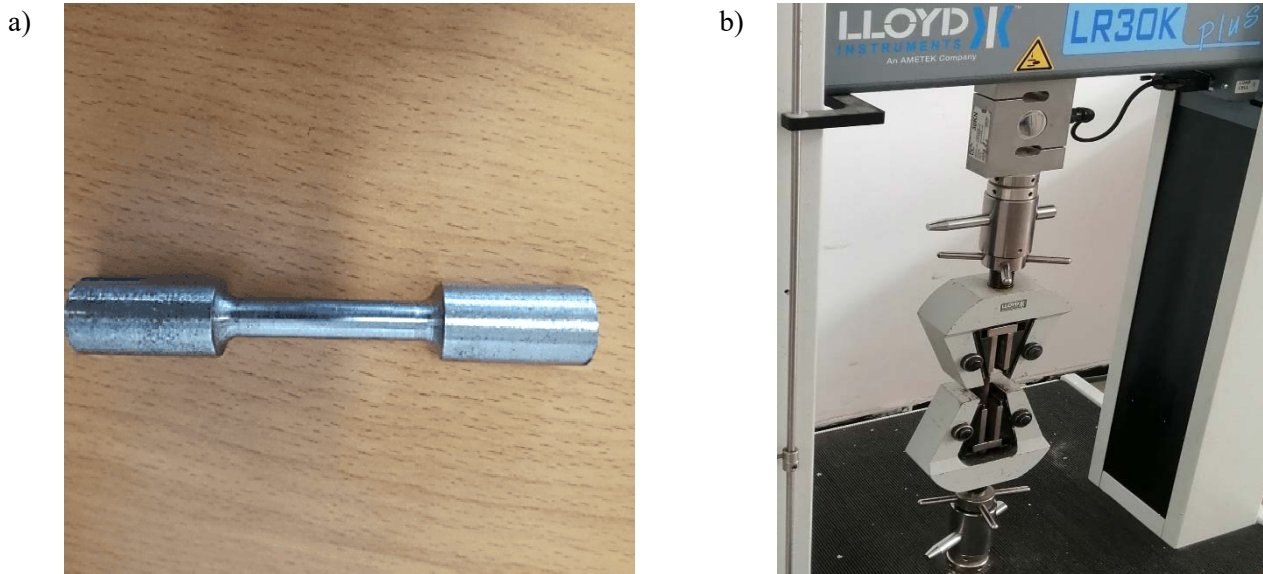


Fig.2. Experimental set-up for the tensile tests: (a) tested specimen; (b) universal testing machine model LR30KPlus.

2.2.2. Vickers hardness tests

The Vickers hardness test was performed to determine the hardness of a material to deformation by using a diamond-shaped indenter to create an impression in the material's surface under a specific load (Fig.3). The hardness is determined from the ratio of the applied load to the surface area of the indentation. The Vickers hardness number (HV) is calculated from the indentation diagonal lengths, making it independent of the indenter size. This test method was conducted in accordance with ISO 6507-1:2005 test standard [18].



Fig.3. Experimental set-up for the Vickers hardness tests.

2.3. Calculation of the shear stress of the bollard under imposed loads

Considering the bollard's shape and dimensions, which experienced failure under external loading (as shown in Fig.4), mechanical analysis and numerical modelling were conducted. These aimed to assess the mechanical response of the most stressed regions under the applied load and to confirm whether the chosen steel grade for the bollard meets the maximum stress tolerance. To achieve this, we used numerical simulations in Mathcad (version 14) and modelling in Catia V5.

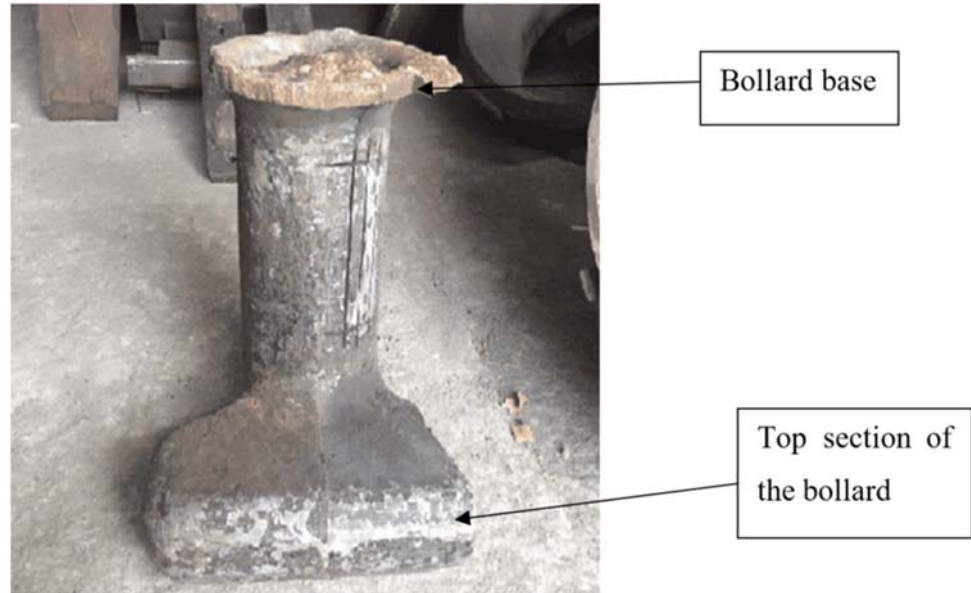


Fig.4. Tested A60 steel bollard.

2.3.1. Numerical simulations in Mathcad

By considering the bollard as a hollow cylinder fixed at its base and subjected to a concentrated load at its end, it can be theoretically demonstrated that the maximum tensile stress due to the combined effect of bending and tension is located at the base of the bollard. This maximum stress occurs when the loading direction is perpendicular to the axis of the cylinder. The figure below illustrates an example of such a configuration.

Using Mathcad 14 simulation software, the variation of the aforementioned tensile stresses with respect to the loading direction is depicted in the figure below under a maximum load of *100 tons*, with the actual dimensions taken from the bollard, as follows:

$$D = 268 \text{ mm (Outer diameter),}$$

$$d = 220 \text{ mm (Inner diameter),}$$

$$L = 380 \text{ mm (The height from the base of the bollard to the upper end).}$$

With reference to Fig.5, the internal mechanical resistance and bending moments were calculated as a function of the angle of force application. We can express shear effort at the base of the bollard:

$$T_y(x) = F \sin(\alpha_i), \quad (2.1)$$

α_i represents the angle of force application in radians with respect to the cylinder axis ($i = 0...; 90$).

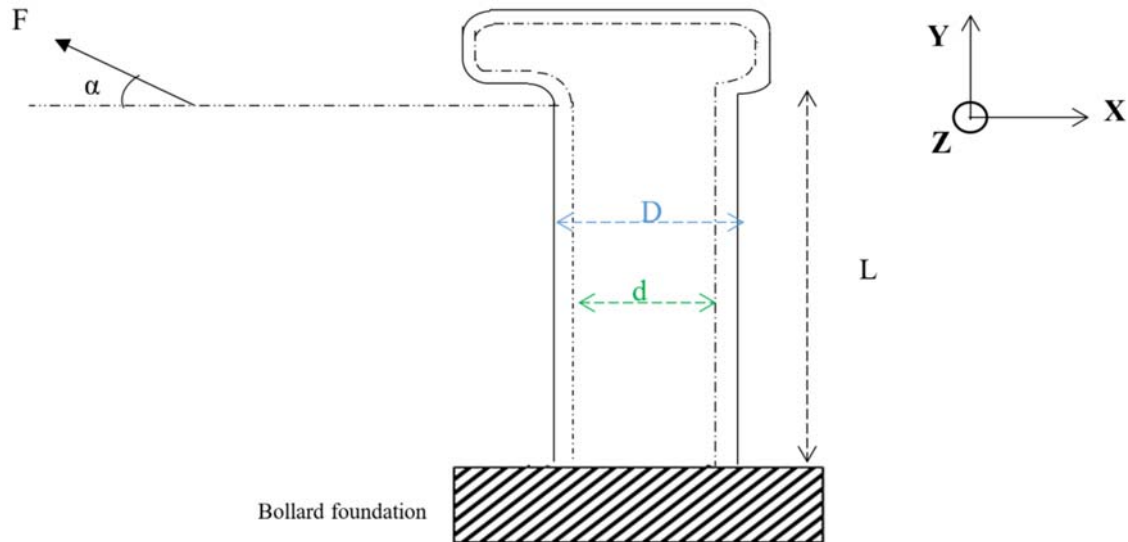


Fig.5. Schematic configuration of the tested bollard.

The normal effort at the bollard's base can also be expressed as follows [19]:

$$N(x) = -F \cos(\alpha_i) . \quad (2.2)$$

We can express the flexural moment at the base of the bollard with this equation [19]:

$$M_{f(x)} = Fx \sin(\alpha_i) . \quad (2.3)$$

From these equations, the tensile stress σ_{TNi} and the bending stress σ_{fNi} are given by the following expressions [19]:

$$\sigma_{TNi} = \frac{4F \sin(\alpha_i)}{\pi(D^2 - d^2)} , \quad (2.4)$$

$$\sigma_{fNi} = LF \sin(\alpha_i) D \frac{32}{\pi(D^2 - d^2)} . \quad (2.5)$$

Based on the last two equations, the total stress generated at the base of the terminal, σ_{Ni} , is therefore expressed by this equation [19]:

$$\sigma_{Ni} = \frac{4F \cdot \sin(\alpha_i)}{\pi(D^2 - d^2)} + LF \sin(\alpha_i) D \frac{32}{\pi(D^2 - d^2)} . \quad (2.6)$$

The shear stress is defined by this equation [19]:

$$\tau_{xy} = Tyi \frac{Q_{\max}}{bI_C} \quad (2.7)$$

where:

b : loaded thickness of the bollard,

I_C : the moment of inertia of the entire cross-sectional area with respect to the neutral axis,

Q_{max} : the maximum statical moment in the cross-section,

b , I_C and Q_{max} are given by:

$$b = D_{ext} - d_{int}, \quad (2.8)$$

$$I_C = \frac{\pi \left[\left(\frac{D}{2} \right)^4 - \left(\frac{d}{2} \right)^4 \right]}{4}, \quad (2.9)$$

$$Q_{max} = \frac{2 \left[\left(\frac{D}{2} \right)^3 - \left(\frac{d}{2} \right)^3 \right]}{3}. \quad (2.10)$$

Referring to Eqs 2.6 and 2.7, the maximum shear stress is given by this equation [19]:

$$\tau_{max i} = \sqrt{\left(\frac{\sigma_{Ni}}{2} \right)^2 + (\tau_{xy})^2}. \quad (2.11)$$

The maximum shear stress is determined by Mohr's method [20], a graphical approach to finding the principal stresses and maximum shear stress in a 2D stress state.

2.3.2. Modelling on Catia v5

In order to examine the areas most affected by the bollard's loading, a numerical modelling was conducted under the same service conditions with a *100 ton* load (Fig.6). Assuming that the position of the anchored zone is located approximately *100 mm* from the base of the bollard (data approximately extracted from the sample that experienced failure).

Table 3. Mechanical properties of the A60 steel bollard used in numerical modelling.

Young's modulus (GPa)	230
Poisson's ratio	0.266
Density (kg/m ³)	7860
Yield strength (MPa)	355
Ultimate tensile strength (MPa)	639

Von Mises constraint is widely used to predict terminal failure by Catia software numerically. It serves as a failure criterion, indicating the probability of failure if the tensile strength is exceeded. This constraint simplifies calculations by providing a single value to compare to the resistance. Compared to normal and shear stresses, it effectively captures their combined effect under complex stress states [21].

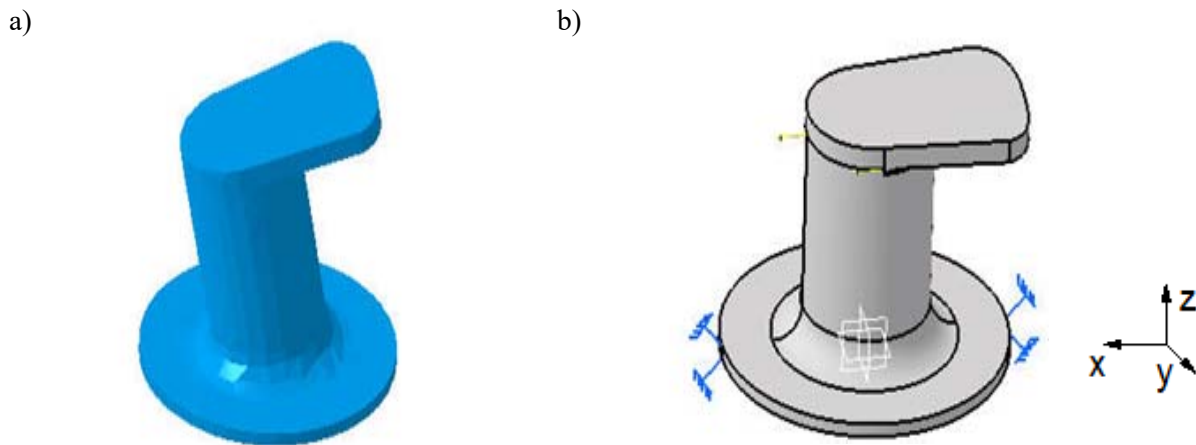


Fig.6. Numerical model developed for modelling: (a) FE model developed for A60 steel bollard. (b) schematic model with boundary conditions.

3. Results analysis

3.1. Characterization tests of bollard steel

3.1.1. Tensile tests

The typical stress-strain curve obtained from tensile tests is shown in the following figure and the obtained values of mechanical properties are summarized in Tab.4:

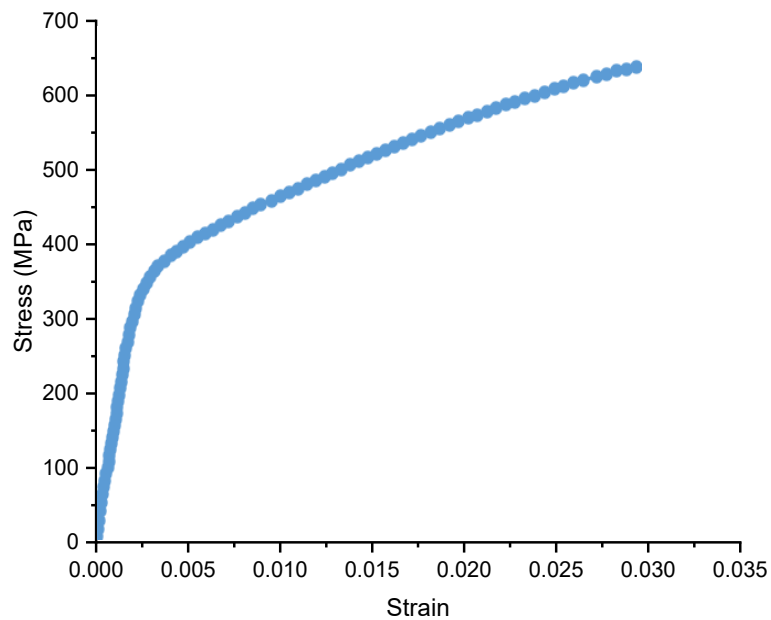


Fig.7. Stress-strain curves obtained from tensile testing of the A60 steel bollard tested.

In reference to the data specified by the standards below, the mechanical properties of the steel in question are in accordance with current standards.

Table 4. Mechanical properties obtained from the stress vs strain curve.

	Tensile strength $R_m (N / mm^2)$	Yield strength $R_e (N / mm^2)$
The value	327	639

3.1.2. Hardness tests

The average hardness obtained from a sample taken from the bollard is 224 HV (average of 5 measurements).

3.2. Calculation of the shear strength of the bollard under imposed loads

3.2.1. Numerical simulation on Mathcad 14

Using Mathcad 14 simulation software, the variation of the tensile stress σ_{TN} , the bending stress σ_{fN} and the total stress generated σ_N as a function of the angle of force application is shown in Fig.8 under a maximum load of 100 tons and with the actual dimensions taken from the bollard.

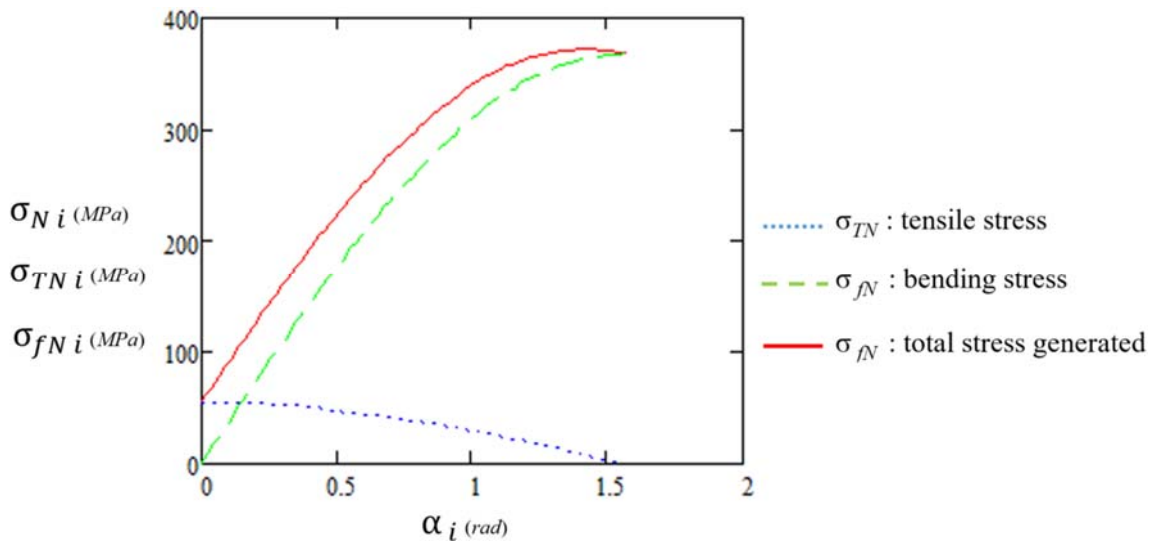


Fig.8. Evolution of the stresses as a function of the direction of loading.

Under the loading conditions, the maximum stress reached at the base of the bollard is approximately 368 MPa, which exceeds the yield strength of material grade A60 (E335).

Figure 9 presents the variation of the maximum shear stress τ_{max} as a function of the angle of force application. Regarding shear resistance under service conditions, it is shown that the maximum shear stress generated due to the shearing effect resulting from the bending of the cylinder, as determined from the construction of the Mohr's circle, is approximately 214 MPa and is achieved at the base of the bollard. Its variation with respect to the loading direction is illustrated in the figure below.

Furthermore, by referring to the bibliographic data that allows estimating the practical shear yield stress of the material based on the knowledge of the tensile yield strength, it is observed that this limit is approximately $0.7 R_e$ for steels with a tensile yield strength ranging from 320 MPa to 500 MPa. Thus, for A60 steel, this limit is 234 MPa, which closely matches the value estimated by Mathcad 14 without any safety factor.

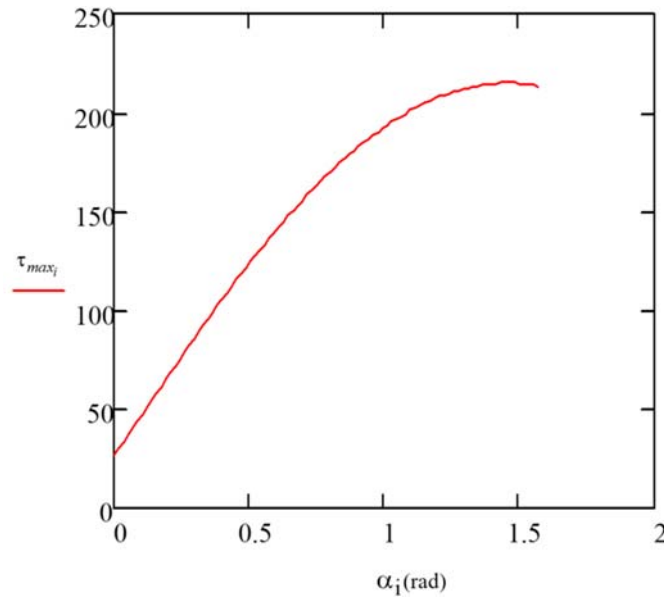


Fig.9. Evolution of the maximum shear stress as a function of the direction of loading.

3.2.2. Modelling on Catia v5

The simulation results, presented in Fig.9, illustrate the Von Mises stress distribution of the A60 steel bollard under a 100 ton load. The examination of the results obtained clearly confirms the theoretical approach conducted in Mathcad 14, which indicates that the most stressed areas are indeed concentrated at the base of the bollard, and the equivalent Von Mises stress, which is approximately 486 MPa, significantly exceeds the allowable maximum elastic limit of the A60 bollard material (Fig.10).

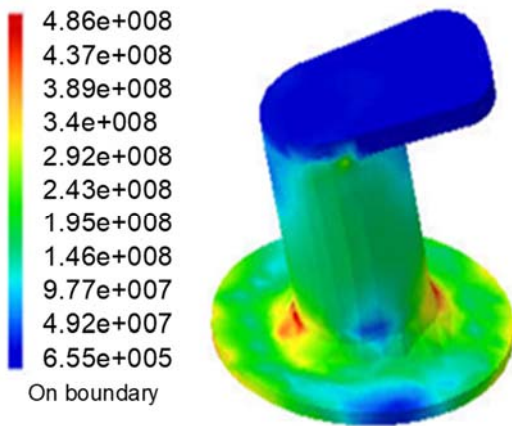


Fig.10. Von Mises stress distribution of the A60 steel bollard under a 100 ton load.

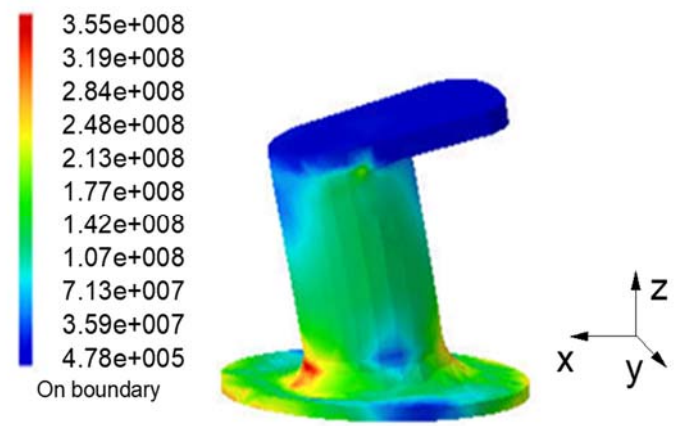


Fig.11. Von Mises stress distribution of the A60 steel bollard under a 73 ton load.

Furthermore, to verify the maximum permissible load (without any safety factor) that would generate a Von Mises stress equivalent to the allowable material elastic limit in question, modelling with the same dimensions revealed that this load is around 73 tons. Beyond this load, ruptures in areas similar to those observed on the damaged bollard are imminent. Figure 11 provides the modelling report obtained for a 73 ton load.

4. Conclusion

After subjecting the bollard to characterization, simulation, and numerical modeling tests based on the dimensions derived from the failed sample, it was noted that the mechanical characteristics of the steel comprising the bollard align with those of A60 steel grade. Nevertheless, when considering the actual dimensions and a 100 ton load, the maximum tensile and shear stresses surpass the permissible elastic limit of the material. Additionally, the Von Mises stress substantially exceeds the allowable elastic limit without incorporating any safety factor, signifying an impending risk of failure for the bollard under a 100 ton load.

Furthermore, considering the existing dimensions of the identified bollard, it is determined that its maximum load-bearing capacity without incurring damage is limited to 73 tons, devoid of any safety margin. To mitigate the risk of damage when subjected to a 100 ton load, it is recommended to reassess the bollard's design. This involves augmenting the thickness of the cylindrical segment and implementing a safety factor of at least 1.5.

Data availability statement

The datasets produced and analyzed in the present study can be obtained from the corresponding author upon a reasonable request.

Nomenclature

$T_y(x)$ – shear effort

α_i – angle of force application in radians with respect to the cylinder axis ($i = 0...;90$)

$N(x)$ – normal effort

$M_f(x)$ – flexural moment at the base of the bollard with this equation

σ_{TNi} – tensile stress

σ_{fNi} – bending stress

σ_{Ni} – total stress generated at the base of the terminal.

τ_{xy} – shear stress

b – loaded thickness of the bollard

I_C – moment of inertia of the entire cross-sectional area with respect to the neutral axis.

Q_{max} – the maximum statical moment in the cross-section.

References

- [1] Cho S.-R., Choung J., Oh C.-M., Lee K.-S. and Kim J.-Y. (2010): *Ultimate load capacities of mooring bollards and hull foundation structures.*– Ocean Eng., vol.37, No.8-9, pp.770-776, doi: 10.1016/j.oceaneng.2010.02.011.
- [2] Roberts C.M. and Skalaski R.P. (2016): *Case study: bollard load testing at US naval facilities.*– Ports, pp.340-350.
- [3] Ravaliya N.R., Kumar S. and Gupta P.K. (2023): *Finite element analysis of hollow circular steel tube subjected to lateral impact load: a comprehensive study.*– J. Fail. Anal. Prev., vol.23, No.5, pp.2275-2294, doi: 10.1007/s11668-023-01778-6.
- [4] Campbell L.A., Butler J.A. and Donaldson R.J. (2021): *Mooring line failures: Considerations for the installation of barrier protection.*– Australasian Coasts & Ports 2021, Te Oranga Takutai, Adapt and Thrive: Te Oranga Takutai, Adapt and Thrive, New Zealand Coastal Society Christchurch, NZ, 2022, pp.230-235.
- [5] Maduliati S., Ngo T.D., Tran P. and Lumantarna R. (2015): *Performance of hollow steel tube bollards under quasi-static and lateral impact load.*– Thin-Walled Struct., vol.88, pp.41-47, doi: 10.1016/j.tws.2014.11.024.

- [6] Daramola O., Adewuyi B. and Oladele I. (2011): *Corrosion behaviour of heat treated rolled medium carbon steel in marine environment.*– J. Miner. Mater. Charact. Eng., vol.10, No.10, pp.888-903.
- [7] Sotoodeh K. (2021): *A review and analysis of industrial valve material failures due to corrosion and proposals for prevention measures based on industrial experiences in the offshore sector of the oil and gas industry.*– J. Fail. Anal. Prev., vol.21, No.1, pp.261-267, doi: 10.1007/s11668-020-01064-9.
- [8] Khadom A.A. (2015): *Protection of steel corrosion reaction by benzotriazoles: a historical background.*– J. Fail. Anal. Prev., vol.15, pp.794-802, doi: 10.1007/s11668-015-0043-4.
- [9] Wu L., Xiang Z., Shu D., Liu M., Yang J. and Li M. (2023): *Dynamic inversion model of the mooring force on a floating bollard of a sea lock.*– J. Mar. Sci. Eng., vol.11, No.7, p.1374, doi: 10.3390/jmse11071374.
- [10] Dawson H. and Tennant D. (2008): *Inelastic dynamic finite-element design of bollard systems to impact loading.*– Structures Congress 2008: Crossing Borders, pp.1-10. doi: 10.1061/41016(314)152.
- [11] Hu B. and Li G.-Q. (2016): *Maximum impact force of truck frontal crashing into antiram bollard systems.*– J. Struct. Eng., vol.142, No.12, p. 04016125, doi: 10.1061/(ASCE)ST.1943-541X.0001612.
- [12] Roberts C. M. (2022): *Mooring hardware load testing an industry update.*– Ports 2022, pp.73-80.
- [13] Wu L., Xiang Z., Shu D., Liu M., Yang J. and Li M. (2023): *An intelligent monitoring system for the force characteristics of floating bollards in a ship lock.*– J. Mar. Sci. Eng., vol.11, No.10, p.1948, doi: 10.3390/jmse11101948.
- [14] Pin Y., Weili W., Guoping D., Jianxin L. and Zhiqiang L. (2022): *Safety monitoring of mooring bollard structure based on optical fiber sensing technology.*– 5th World Conf. on Mech. Eng. and Intelligent Manufacturing (WCMEIM), IEEE, pp.604-609. doi: 10.1109/WCMEIM56910.2022.10021362.
- [15] Sydorenko I., Tonkonogyi V., Semenyuk V., Lingur V. and Zhang Y. (2022): *Stress-strain state of the floating bollard's structure for a shipping gateway.*– Advances in Design, Simulation and Manufacturing, pp.23-32, doi: 10.1007/978-3-031-06044-1_3.
- [16] Zhang Y., Sydorenko I., Prokopovych I., Zhang Y. and Voronenko S. (2021): *Simulation of a floating bollard of a ship lock by the finite element method.*– Odes'kyi Politechnichnyi Universytet, No.1, pp.5-12.
- [17] Aegerter J., Kühn H.-J., Frenz H. and Weißmüller C. (2011): *EN ISO 6892-1: 2009 tensile testing: initial experience from the practical implementation of the new standard.*– Mater. Test., vol.53, No.10, pp.595-603, doi: 10.3139/120.110269.
- [18] AENOR UNE-EN ISO 6507-1 (2006): *Metallic Materials. Vickers Hardness Test. Part 1: Test Method (ISO 6507-1: 2005).*
- [19] Bourahla N. (2005): *Strength of Basic Materials (in French).*– Univ. Saad Dahlab Blida Ed., GEOTEC, p.290.
- [20] Balmer G. (1952): *A general analysis solution for Mohr's envelope.*– Proc. ASTM, pp.1260-1271.
- [21] Mises von R. (1913): *Mechanics of solid bodies in the plastic-deformable state (in German).*– Nachrichten von Ges. Wiss. zu Gött. Math.-Phys. Kl., vol.1913, pp.582-592.

Received: February 14, 2024

Revised: April 29, 2024